Dalton Transactions

ROYAL SOCIETY OF CHEMISTRY

PAPER

View Article Online
View Journal | View Issue

Cite this: *Dalton Trans.*, 2020, **49**, 16736

Alkaline earth-organic frameworks with amino derivatives of 2,6-naphthalene dicarboxylates: structural studies and fluorescence properties†

Stavros A. Diamantis, [a] Antonios Hatzidimitriou,[a] Alexios K. Plessas, [b] Anastasia Pournara,[c] Manolis J. Manos, [c] Giannis S. Papaefstathiou *[b] and Theodore Lazarides *[a]

Alkaline earth metal ion organic frameworks (AEMOFs) represent a relatively underexplored subcategory of metal–organic frameworks (MOFs). In this contribution, we present the synthesis and structural study of the new MOFs **1–8** based on the alkaline earth ions Mg^{2+}, Ca^{2+}, Sr^{2+} and Ba^{2+} and the amino substituted bridging ligands 4-aminonaphthalene-2,6-dicarboxylate ($ANDC^{2-}$) and 4,8-diaminonaphthalene-2,6-dicarboxylate ($DANDC^{2-}$). Compounds **1**, **5**, **6**, **7** and **8** constitute rare examples of three-dimensional MOFs which feature square planar M_4 secondary building units (SBUs) surrounded by eight bridging ditopic ligands. The underlying topology of MOFs **1**, **5**, **7** and **8** conforms to the 4-c **pcb** net which can be simplified to the 8-c **bcu** net, while **6** adopts the 4-c **lta** net which simplifies to the 8-c **reo** net. To the best of our knowledge these are the first examples of MOFs of their structural types formed by linear dicarboxylates instead of trigonal tricarboxylates or tetrahedral tetracarboxylates. Compounds **2**, **3** and **4** also feature three dimensional networks with linear rod-shaped SBUs with the Ba^{2+} MOF **3** displaying an **sra** rod-net and MOFs **2** and **4** showing very complex rod-nets with so far unique topologies. Fluorescence studies revealed that the free ligands exhibit strong blue-green emission displaying considerable positive solvatochromism thereby pointing towards charge transfer excited states involving the shift of electron density from the amino groups to the aromatic core. Correspondingly, the MOFs display ligand based fluorescence with small differences in emission maxima possibly attributable to the difference in the charge density of the metal ions combined with the different environments around ligands in the crystal structures.

Received 24th September 2020,
Accepted 21st October 2020

DOI: 10.1039/d0dt03325a

rsc.li/dalton

Introduction

Metal–organic frameworks (MOFs) constitute a unique class of porous (or potentially porous) materials which are characterized by two or three-dimensional open network structures consisting of nodes in the form of metal centres (either single ions or clusters) which are interconnected by bridging polydentate organic ligands.[1–3] MOFs are intensely investigated due to their structural and functional variety which makes them attractive for a plethora of applications such as gas storage and separation,[4–8] catalysis,[9–15] ion sorption and exchange[14,16–19] and more recently as chemical sensors.[16,20–26]

In comparison to d-block and rare earth metal ions, research on alkaline earth MOFs (AEMOFs) is still on a rather preliminary level.[27] The closed-shell electronic structure of alkaline earth ions results in their MOFs exhibiting ligand-based fluorescence[28–30] which, in the cases where ligands contain suitable functional groups, can prove to be of interest for possible sensing applications.[31–33] In addition, there are examples of AEMOFs which show promising gas separation,[34,35] catalytic[36,37] and electrical properties.[38–42] Amino functionalized aromatic dicarboxylates are of particular interest for MOF synthesis as they can lead to materials with increased CO_2 adsorption[43] and favorable fluorescence[44] and photocatalytic[45–48] properties. However, the chemistry of amino functionalized MOFs is largely dominated by the

[a]*Laboratory of Inorganic Chemistry, Department of Chemistry, Aristotle University of Thessaloniki, Thessaloniki, 54124, Greece. E-mail: tlazarides@chem.auth.gr*
[b]*Laboratory of Inorganic Chemistry, Department of Chemistry, National and Kapodistrian University of Athens, Panepistimiopolis, Zografou 15771, Greece. E-mail: gsppaef@chem.uoa.gr*
[c]*Laboratory of Inorganic Chemistry, Department of Chemistry, University of Ioannina, Ioannina 45110, Greece*

† Electronic supplementary information (ESI) available: Ligand and AEMOFs synthesis, NMR spectra and ESI-MS data of the H_2DANDC ligand, thermal analyses data, single crystal and powder X-ray diffraction data, excitation and absorption UV-vis spectra. CCDC 2033666–2033673. For ESI and crystallographic data in CIF or other electronic format see DOI: 10.1039/d0dt03325a

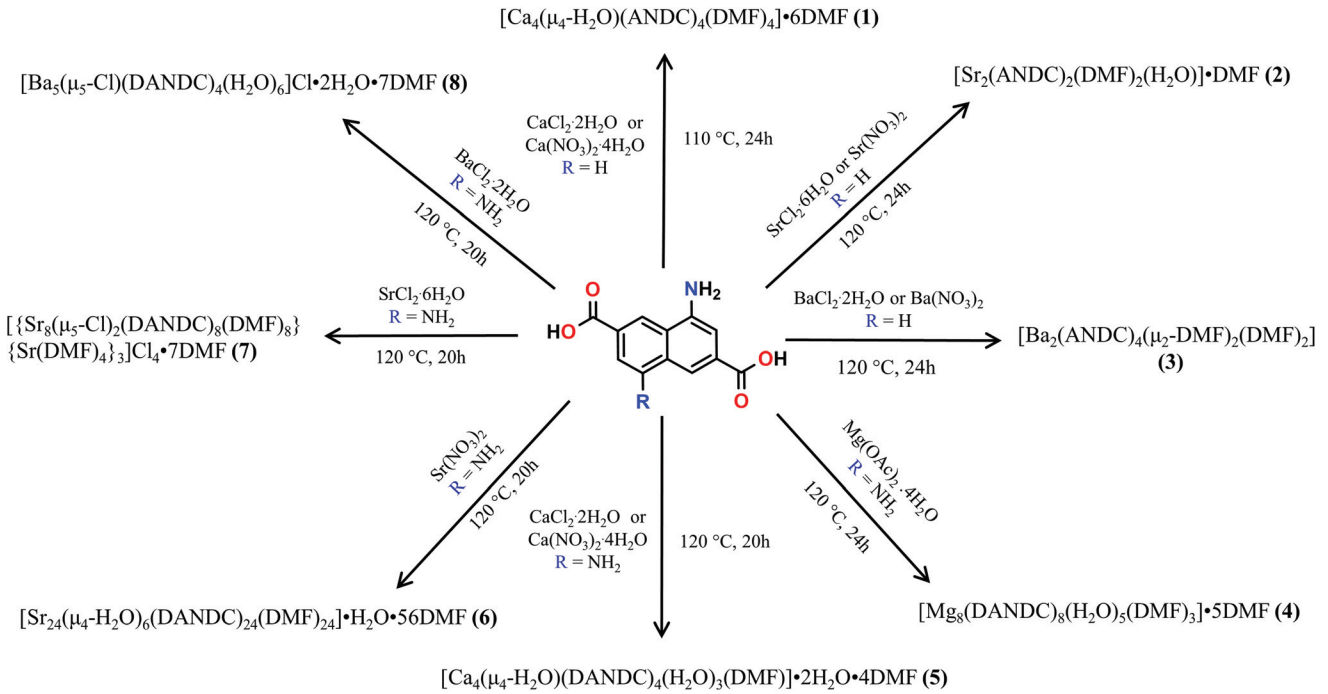

Scheme 1 Synthetic routes leading to compounds **1–8**.

2-amino-1,4-benzenedicarboxylate (NH_2BDC^{2-}) and 5-amino-1,3-dicarboxylate ligands and their derivatives[43,49] with only relatively few examples involving ligands with longer naphthalene or biphenyl spacers.[47,50–58]

In this contribution, we report the synthesis and structural and photophysical study of AEMOFs **1–8** (Scheme 1) which are based on the amino-substituted dicarboxylic bridging ligands 4-aminonaphthalene-2,6-dicarboxylate ($ANDC^{2-}$)[55] and 4,8-diaminonaphthalene-2,6-dicarboxylate ($DANDC^{2-}$). A synthesis of the latter ligand through the catalytic hydrogenation of 4,8-dinitro-2,6-naphthalene dicarboxylic acid[59] is also reported here. The AEMOFs form open three-dimensional frameworks and display remarkable structural features with, in some cases, unique network topologies and metal secondary building units (SBUs) ranging from infinite rods to rarely observed tetranuclear square planar clusters.[60–64] The UV–vis absorption and fluorescence spectra of the free ligands H_2ANDC and H_2DANDC show significant solvatochromism which is consistent with charge transfer excited states. The corresponding AEMOFs exhibit ligand-based blue-green fluorescence at room temperature.

Results and discussion

The reactions of alkaline earth metal salts with H_2ANDC and H_2DANDC ligands in dimethylformamide (DMF) containing 10% (v/v) water at 110–120 °C afforded a series of crystalline products **1–8**, the formulas of which, as determined by single crystal X-ray crystallographic analysis, can be seen in Scheme 1. All the compounds were found to possess three-dimensional network structures which are described in detail in the following sections. Tables containing crystallographic details and selected bond angles and distances for each structure can be found in ESI (Tables S1–10†).

Crystal structures of 1, 5, 7 and 8

These MOFs crystallize in the tetragonal *I*4/*m* space group (Tables S1 and 2†) and their structures are based on tetranuclear SBUs $M_4(COO)_8$ (M = Ca for **1** and **5**; Sr for **7**; Ba for **8**), with the metal ions arranged on the corners of a square and being held together by eight chelating, bridging μ_2–η^2:η^1 carboxylate groups four of which are above and four below the square plane. It is worth noting that, square M_4 SBUs are relatively rare compared to those where the four metal atoms are in a tetrahedral arrangement and have mainly been observed with divalent transition metal ions such as Cu[62] and Cd[63] and trivalent lanthanides.[64] To the best of our knowledge, there is only one example of a MOF with a square Ca_4O SBU which involves the tetrahedral tetracarboxylic ligand methanetetrabenzoate (MTB).[34,60] In our compounds, the centre of the M_4 square is occupied by a disordered water molecule in the cases of the Ca^{2+} MOFs **1** and **5** (Fig. 1A) or by a chloride anion in the cases of the Sr^{2+} and Ba^{2+} MOFs **7** and **8** (Fig. S14A† and Fig. 1C respectively). Each of the four M^{2+} ions is eight coordinated by six carboxylic oxygen atoms, one water molecule (**1** and **5**) or one Cl^- ion (**7** and **8**) and one terminal DMF (**1**, **5** and **7**) or water (**8**) ligand. The coordination polyhedron about the metal ion can be best described as a distorted square antiprism. In the cases of the compounds involving the larger Sr^{2+} and Ba^{2+} ions (**7** and **8**), the four bridging carboxylic oxygen

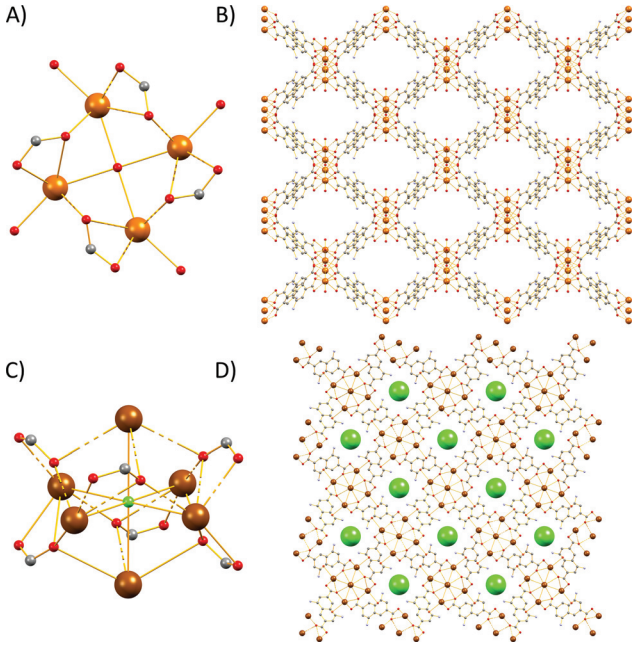

Fig. 1 Representation of the (A) tetranuclear SBU of **1**; (B) three-dimensional structure along the *b* axis of **1**; (C) metal core of **8** and (D) three-dimensional structure along the *c* axis of **8**, the chloride counter-ions are displayed in space-filling mode. H atoms and solvent molecules are omitted for clarity. Colour code: Ca, brown; Ba dark brown; C, gray; O, red; N, blue; Cl, green.

atoms residing above the square M_4 plane, together with their four counterparts residing below the latter, create two oxygen-rich "nests" which are partially occupied by M^{2+} cations thereby creating M_6 octahedra. The extra positive charge which is introduced in **7** and **8** is balanced by Cl^- counter ions which are located in the centre of the M_4 square plane and in the cavities of the MOFs. It is worth mentioning that in the case of the smaller Sr^{2+} ion (**7**) we observe disorder in both the Cl^- anion and the carboxylic oxygen atoms which are involved in bonding with the axial metal ions (Fig. S14†). The distances between the metal ions and the carboxylate oxygens range from 2.252 to 2.882 Å. The bond length between the Ca^{2+} ions and the oxygen atom of the central H_2O molecule were found to be 2.564 and 2.670 Å in **1** and **5** respectively. The considerably larger distances observed in the case of **5** possibly reflect the higher steric demand of the $DANDC^{2-}$ bridging ligand. In the case of **8**, the distance between the metal ions of the M_4 plane and the bridging chloride ions was found to be 3.123 Å. The crystal structures of **7** and **8** are stabilized by strong hydrogen bonds between the amino groups of the dicarboxylate linker and (a) the chloride counter ions (2.393–2.552 Å) and (b) the carboxylate oxygen of a neighboring ligand (2.137–2.158 Å).

The three-dimensional the structures of **1**, **5**, **7** and **8** are formed by M_4 SBUs surrounded by eight dicarboxylate ligands (Fig. 1B and D). It is worth mentioning that the structures of **1**, **5**, **7** and **8** bear close resemblance to that observed in a fluorite-like MOF reported by Kim and co-workers[65] in 2004 which is constructed by square planar Cd_4 SBUs (which are similar to the M_4 SBUs presented here) interconnected by eight tetrahedral tetracarboxylate MTB ligands. To the best of our knowledge, structures **1**, **5**, **7** and **8** represent the first examples of this structural type with a linear dicarboxylate bridging ligand.

From the topological point of view, the M_4 clusters in **1**, **5**, **7** and **8** are surrounded by eight different dicarboxylate ligands (one unique) that connect the central cluster to eight neighboring M_4 clusters (Fig. S15†) The eight carboxylate C atoms around each M_4 cluster form a rectangular prism with distances of ~ 4 to 5 Å. The vertices of the prism are connected through the naphthalene moieties of the ligands (C···C ~ 8 Å) to produce a uninodal 4-coordinate **pcb** network with point symbol $(4^3{\cdot}8^3)$. These MOF have been to found to adopt the exact same topology with other MOFs[66–68] such as such as $[Zn_8(Im)_6(MBIm)_6]^{4-}$,[69] and the hydrogen-bonded assemblies MOC-2[70] and $Co^{(II)}{}_{14}$-MOC.[71] Simplification of the **pcb** network by contracting the eight C atoms of each square prism to their centre of gravity produces a uninodal 8-coordinate **bcu** network with point symbol $(4^{24}{\cdot}6^4)$, which has been observed in many MOFs (Fig. S15†).[72–74]

Crystal structure of 6

The Sr^{2+} MOF **6**, which is not topologically equivalent to **1**, **5**, **7** and **8**, crystallizes in the cubic space group $Fm\bar{3}c$ and its metal SBU is virtually identical to those observed in Ca^{2+} MOFs **1** and **5**. However, it is worth noting that, to the best of our knowledge, **6** constitutes the first example of an SBU consisting of four Sr^{2+} ions in a square planar arrangement. As expected from the larger radius of Sr^{2+}, the Sr–Sr and Sr–O distances within the Sr_4 cluster of **6** are considerably larger than those of **5** (3.814 and 2.697 Å respectively). Similarly to **1**, **5**, **7** and **8**, the basic building unit of **6** is a square prism formed by the eight carboxylate C atoms around each Sr_4 unit with the naphthalene moieties of the eight $DANDC^{2-}$ ligands bridging the Sr_4 SBUs (Fig. 2).

However, in contrast to the above described structures, the underlying network of **6** is different. Owing to the different symmetry of the structure, the orientation and the connectivity of the square prisms is slightly different resulting also in a 4-c net but with the three letter code **lta** and point symbol $(4^3{\cdot}6^2{\cdot}8)$.[75–78] As expected, the simplification of the **lta** net by contracting the eight C atoms of each square prism to their centre of gravity produces a uninodal 8-coordinate **reo** network with point symbol $(3^8{\cdot}4^8{\cdot}5^8{\cdot}6^4)$, which has been observed in many MOFs (Fig. S16†).[79–81]

Crystal structure of 2

Compound **2** crystallizes in the monoclinic space group $P2_1/c$ (Table S1†) and features a three-dimensional framework with two crystallographically unique Sr^{2+} ions (Sr1, Sr2). The structure of **2** is based on an infinite twisted rod SBU $[Sr_2(COO)_4(DMF)_2(H_2O)]_\infty$. Both Sr^{2+} ions are eight coordinated and the coordination polyhedron around them is best described as a biaugmented triangular prism. The Sr1 ion is

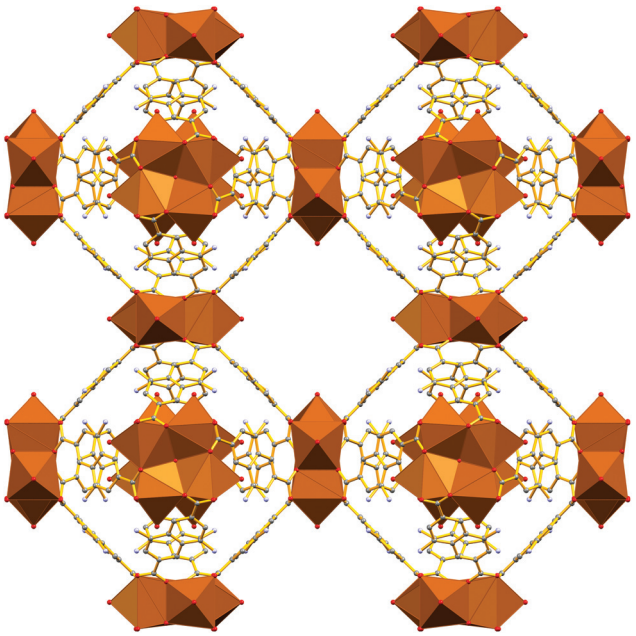

Fig. 2 Representation of the three-dimensional structure of **6**. H atoms and solvent molecules were omitted for clarity. Colour code: Sr, brown; C, gray; O, red; N, blue.

ligated to six carboxylate oxygen atoms, one water molecule and a terminal DMF ligand (Fig. 3). On the other hand, the coordination sphere of Sr2 contains seven carboxylate oxygen atoms and one oxygen atom from a terminal DMF molecule.

The carboxylate groups in **2** bridge the Sr atoms to create a twisted chain (rod) of alternate face and edge-sharing biaugmented triangular prisms running parallel to the *c* axis (Fig. S17†). If we consider the carboxylate C atoms (C1, C12, C13, and C19) as the points of connection, then a corner-sharing ladder of distorted square pyramids forms along the rod. The distorted square pyramids have one more corner linked and their apexes point almost to the same side of the rod. These ladders are further linked by the naphthalene moities of the ligands to create a complex tetranodal network comprising three 5-coordinate and one 7-coordinate node. The point symbol of this net is $(3^3.4^2.5.7^3.8)(3^3.4^2.5^3.6^2)(3^4.4^2.8^4)(3^5.4^4.5^5.6^5.7^2)$ and it is, as expected, unique so far.

Crystal structure of 3

Representation of the SBU and the three-dimensional structure of **3** are shown in Fig. 4. Compound **3** crystallizes in monoclinic space group $P2_1/n$ (Table S1†). The structure of **3** is based on an infinite rod SBU $Ba_2(COO)_4(\mu_2\text{-DMF})_2(DMF)_2$ in which there are two crystallographically unique Ba^{2+} (Ba1, Ba2) ions. Both Ba^{2+} ions are nine-coordinated, with the coordination polyhedron around them being best described as muffin-like. Each Ba^{2+} is ligated to six carboxylate oxygen atoms, two μ_2-brigding DMF molecules and a terminal DMF ligand.

Topologically, the carboxylate groups bridge the Ba1 atoms to create a chain (rod) of alternate edge sharing Ba1 muffins running parallel to the *b* axis (Fig. S18†). A very similar situation is found for the second Ba2 atom, a rod of face sharing Ba2 muffins forms along *b* axis, parallel to the previous Ba1 rod. If we consider the carboxylate C atoms (C1 and C24 for Ba1 and C12 and C13 for Ba2) as the points of connection, then a ladder forms along the Ba1 rod and a second ladder forms along the Ba2 rod. These ladders are further linked by the naphthalene moities of the ligands such that each Ba1 rod being surrounded by four Ba2 rods and *vice versa*. Therefore, a uninodal 4-coordinate network is formed with three-letter code **sra** and point symbol $(4^2{\cdot}6^3{\cdot}8)$. The same **sra** rod-net has been observed in several MOFs.[82–84]

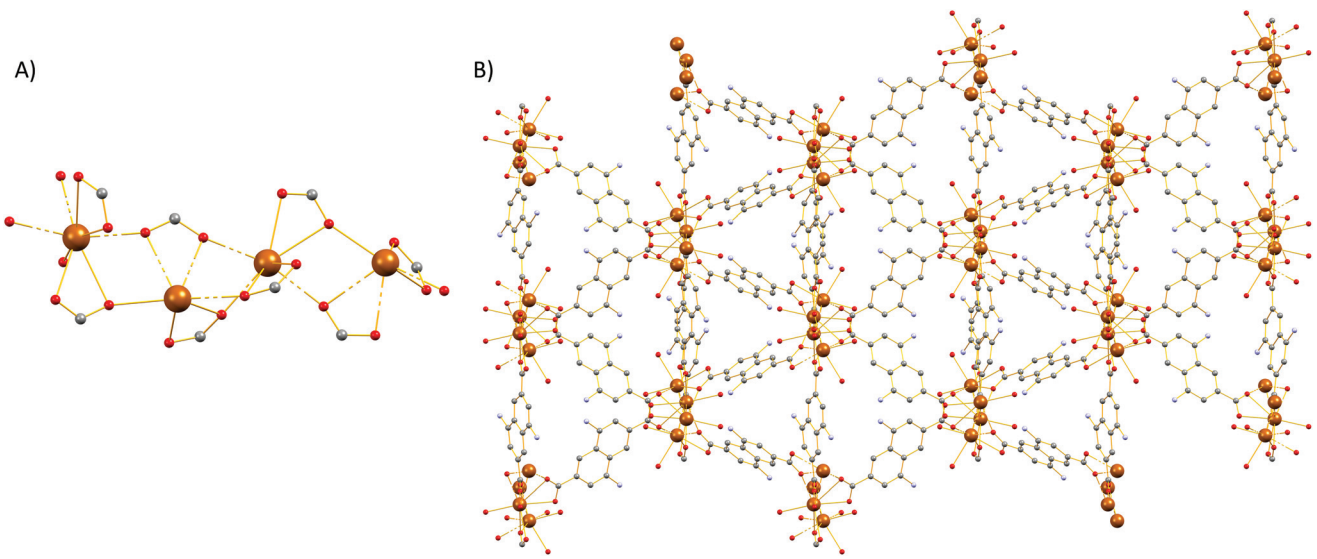

Fig. 3 Representation of the (A) SBU and (B) three-dimensional structure along the *c* axis of **2**. H atoms and solvent molecules were omitted for clarity. Colour code: Sr, brown; C, gray; O, red; N, blue.

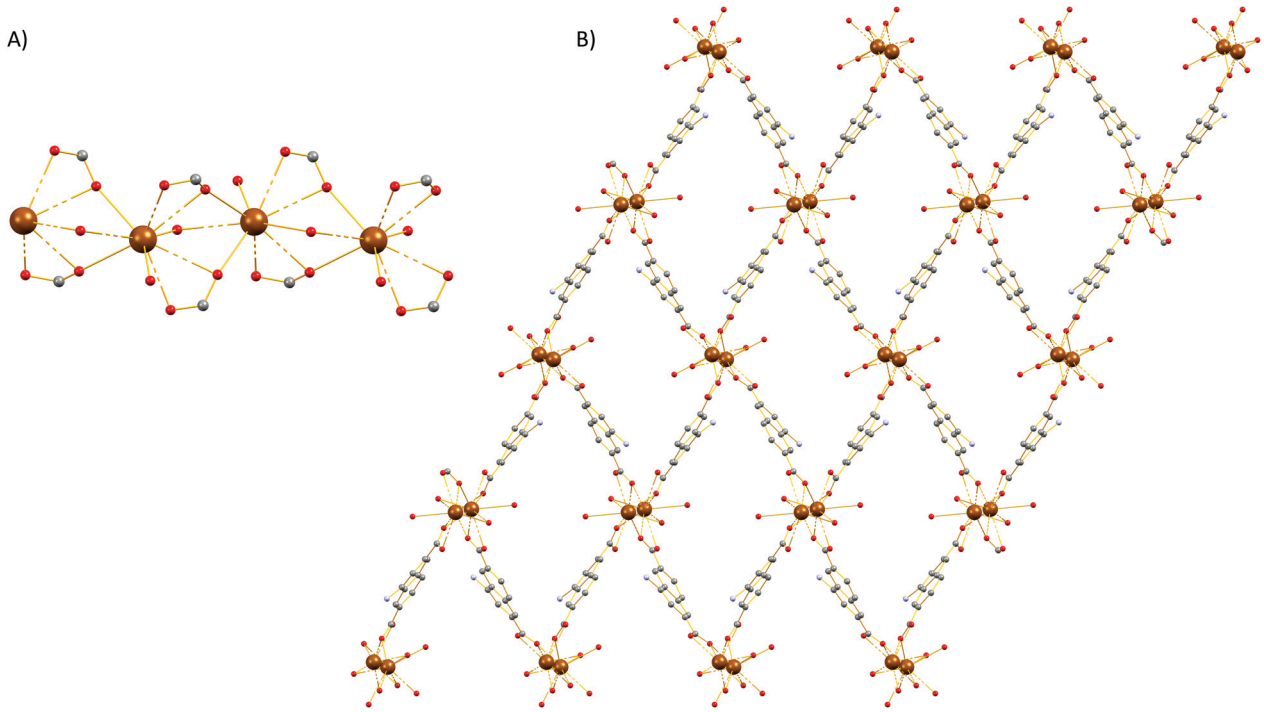

Fig. 4 Representation of the (A) SBU and (B) three-dimensional structure along the *b* axis of **3**. H atoms and solvent molecules were omitted for clarity. Colour code: Ba, brown; C, gray; O, red; N, blue.

Crystal structure of 4

Single-crystal X-ray diffraction reveals that **4** crystallizes in the monoclinic $P2_1/c$ space group (Table S1†). The SBU of **4** consists of an infinite rod $[Mg_2(COO)_4(H_2O)_{1.75}(DMF)_{0.25}]$ unit (Fig. 5A) featuring two crystallographically independent Mg^{2+} ions (Mg1, Mg2). Mg1 is five-coordinated by five oxygen atoms to form a distorted square pyramid in which four oxygen atoms are from the carboxylate groups of the dicarboxylic ligands and another oxygen (O10) is from terminally coordinated solvent and was modeled as originating from a water molecule (75% occupancy) and from the C═O group of a DMF molecule (25% occupancy). On the other hand, Mg2 ion is six-coordinated by oxygen atoms and each of them is ligated with five carboxylate groups which belong to four different carboxylate ligands and one oxygen atom (O9) which was modeled as originating from a coordinated water molecule and from the C═O group of a terminal DMF ligand (50% occupancy). The geometry around Mg2 is best described as a distorted octahedron. The three-dimensional structure of **4** is shown in Fig. 5B. From the topological view, Mg1 and Mg2 are bridged by three carboxylate groups to create a corner sharing dimer. These dimers are further bridged by a syn, anti-carboxylate thus creating a rod along *c* (Fig. S19†). If we consider the carboxylate C atoms (C1, C7, C13, and C19) as the points of connection, then a corner sharing zig-zag chain of distorted trigonal bipyramids forms along the rod. These chains of distorted trigonal bipyramids are further linked by the naphthalene moities of the ligands to create a complex tetranodal network comprising three 5-coordinate and one 7-coordinate node. The point symbol of this net is $(3^5{\cdot}4{\cdot}6^2{\cdot}7^2)_3(3^6{\cdot}6^9{\cdot}7^6)$ and it is, as expected, unique so far.

Thermal stability

The thermal stability of compounds **1–8** was studied by thermogravimetric analysis on a Mettler-Toledo TGA/DSC1 instrument under a N_2 flow of 50 mL min^{-1}. The thermographs of **1–8** (Fig. S20–27†) data show weight losses starting from 25 °C and ending at over 800 °C they involve the removal of the solvent molecules, followed by the collapse of the frameworks above 210 °C.

Photophysical properties

Compounds **1–8** were studied by steady-state fluorescence spectroscopy in the solid state at room temperature. The free ligands H_2ANDC and H_2DANDC were studied by UV–vis absorption and fluorescence spectroscopy in DMF/MeOH mixed solvent systems.

The absorption spectra of the amino substituted ligands show strong absorptions in the UV region which can be assigned to fully allowed $\pi^* \leftarrow \pi$ transitions of the aromatic core (Fig. S30†).[85] The lowest energy absorption signals ($\lambda_{max} \sim$ 400 nm) exhibited by H_2ANDC and H_2DANDC consist of broad peaks of moderate intensities ($\varepsilon \sim 3000\ M^{-1}\ cm^{-1}$) which show only a slight blue shift upon changing the solvent from DMF to methanol (Fig. S31 and 32†). The emission spectra of

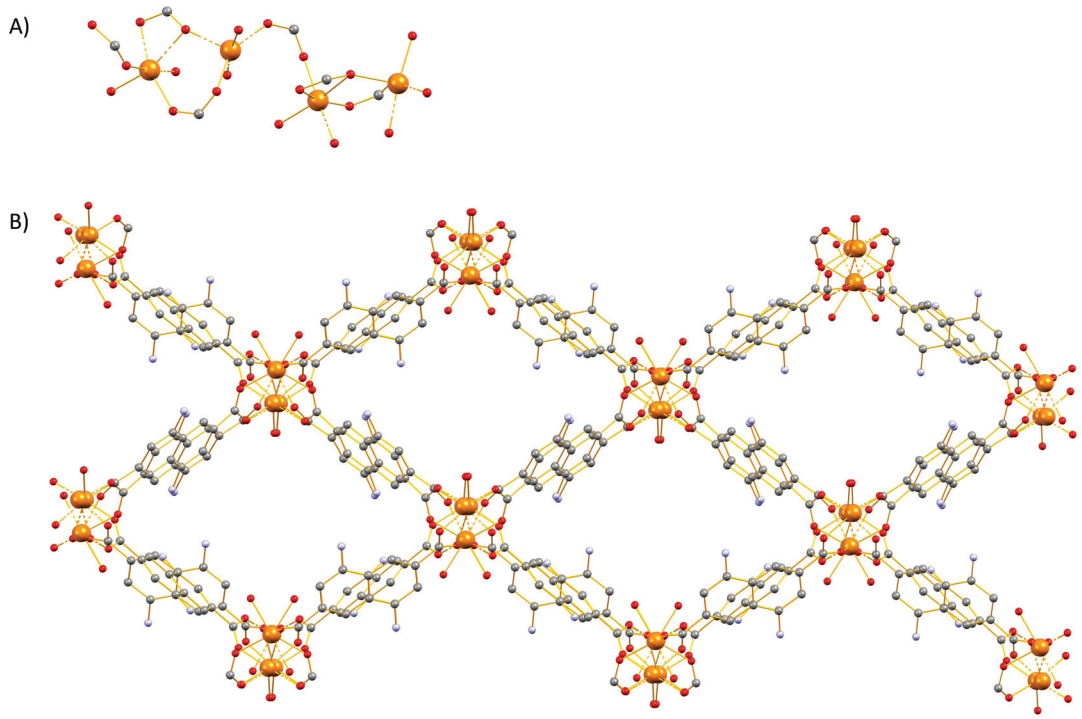

Fig. 5 Representation of the (A) SBU and (B) the three-dimensional structure along the *c* axis of **4**. H atoms and solvent molecules were omitted for clarity. Colour code: Mg, brown; C, gray; O, red; N, blue.

H_2ANDC and H_2DANDC in DMF/MeOH mixtures (ranging from pure DMF to pure MeOH) upon selective excitation at the lowest energy absorption (λ_{exc} = 370 nm) can be seen in Fig. 6 and 7. The excitation spectra (Fig. S33 and 34†) show excellent agreement with the UV–vis absorption spectra in both profile and tendency of the lowest energy absorption feature to undergo a slight blue shift upon increasing the polarity of the solvent system. H_2ANDC and H_2DANDC show similar emission profiles which undergo a significant red shift upon increasing the MeOH content of the solvent system (λ_{max} values shift from 500 to 526 nm for H_2ANDC and from 480 to 520 nm for H_2DANDC in DMF and MeOH respectively. The observed stabilization of the lowest energy ligand-based excited states as the polarity of the medium increases, is consistent with them being of charge transfer nature involving the excitation of an electron in a predominantly amino group orbital to an empty π^* orbital of the aromatic core.[85]

Upon excitation at 370 nm MOFs **1–8** exhibit emission profiles that show good general agreement with those observed for the corresponding ligands (Fig. 8 and 9). This observation

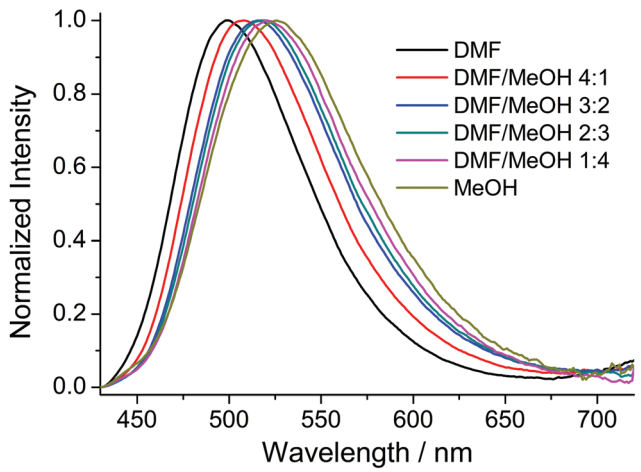

Fig. 6 Emission spectra of the H_2ANDC ligand in DMF/MeOH mixtures (λ_{exc} = 370 nm).

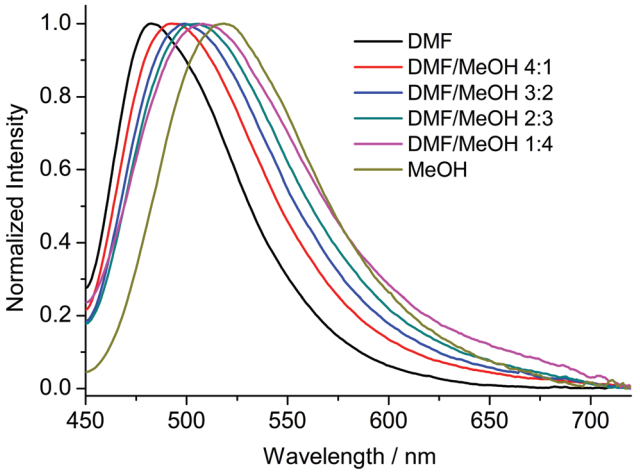

Fig. 7 Emission spectra of the H_2DANDC ligand in DMF/MeOH mixtures (λ_{exc} = 370 nm).

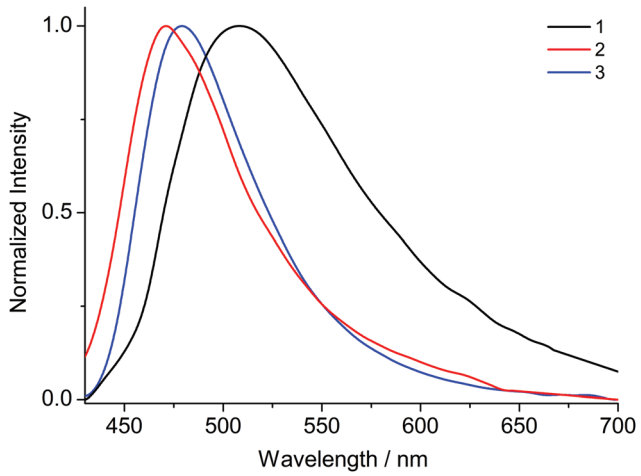

Fig. 8 Solid state emission spectra of **1–3** (λ_{exc} = 370 nm).

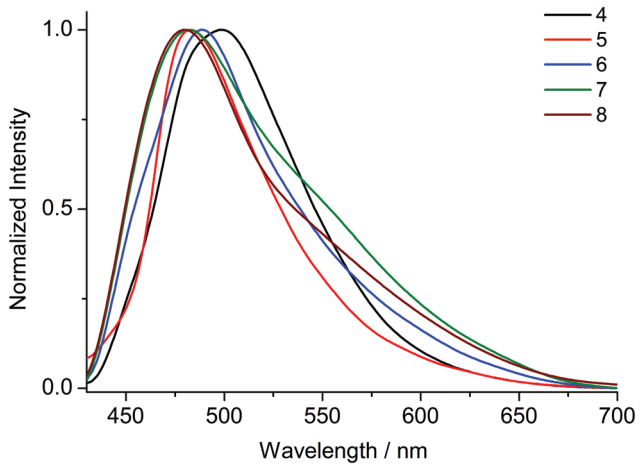

Fig. 9 Solid state emission spectra of **4–8** (λ_{exc} = 370 nm).

combined with the spectroscopically inert closed shell alkaline earth cations, confirms that the observed fluorescence is ligand-based. In the cases of the $ANDC^{2-}$-based MOFs **1**, **2** and **3** (Fig. 8), the emission maxima are at 509, 472 and 479 nm respectively. The significant red shift in the emission maximum of **1** compared to those of **2** and **3** can be possibly be assigned to a combination of structural and electrostatic factors related to the higher charge density of the Ca^{2+} ion relative to Sr^{2+} and Ba^{2+}.[33] The stronger electron withdrawing effect of the Ca^{2+} cation possibly induces a stabilizing effect on the π^* orbitals of the aromatic core of $ANDC^{2-}$ thereby decreasing the energy of the intraligand charge transfer transition. Additionally, as demonstrated by the solvatochromism exhibited by the uncoordinated ligands, the emission energies of the organic linkers also depend on the immediate environment around their chromophores such as the existence and relative strength of hydrogen boding interactions. As a result, the observed emission energies are possibly the result of a finely balanced interplay between the above-mentioned factors. This is also reflected in the cases of the $DANDC^{2-}$-based MOFs **4–8** (Fig. 9) (**4** λ_{em} = 499 nm; **5** λ_{em} = 489 nm; **6** λ_{em} = 483 nm; **7** λ_{em} = 482 nm; **8** λ_{em} = 480 nm) which generally show a less pronounced variation in their emission maxima.[28]

Conclusion

In summary, a series of eight alkaline earth MOFs **1–8** has been isolated by reacting chloride and nitrate salts of Mg^{2+}, Ca^{2+}, Sr^{2+} and Ba^{2+} with mono- and di-amino naphthalene dicarboxylate linkers. Five of the compounds, **1** and **5–8**, display rarely encountered square M_4 SBUs with either a disordered water molecule (**1**, **5**, **6**) or a chloride ion (**7** and **8**) in the centre. In the cases of the chloride-bridged **7** and **8**, the positions above and below the centre of the square plane are partially occupied by M^{2+} ions thereby creating M_6 octahedra. MOFs **1**, **5**, **7** and **8** form 4-c **pcb** nets which can be simplified to the 8-c **bcu** net, while **6** adopts the 4-c **lta** net which simplifies to the 8-c **reo** net. In contrast, MOFs **2**, **3** and **4** also feature three dimensional networks with linear rod-shaped SBUs with the Ba^{2+} MOF **3** displaying an **sra** rod-net and MOFs **2** and **4** showing very complex rod-nets with so far unique topologies. Preliminary fluorescence spectroscopy studies showed that all the compounds show blue green fluorescence with profiles which bare close resemblance to the charge transfer-type emission of the free ligands. Further work exploring the coordination chemistry of amino substituted dicarboxylates and their potential applications as fluorescent sensors and light emitters is ongoing in our laboratory.

Author contributions

The manuscript was written through contributions of all authors. All authors have given approval to the final version of the manuscript.

Conflicts of interest

There are no conflicts to declare.

Acknowledgements

SD thanks the State Scholarships Foundation (IKY) for a doctoral research scholarship. This research is co-financed by Greece and the European Union (European Social Fund – ESF) through the Operational Programme "Human Resources Development, Education and Lifelong Learning" in the context of the project "Strengthening Human Resources Research Potential *via* Doctorate Research – 2nd Cycle" (MIS-5000432), implemented by the State Scholarships Foundation (IKY). GSP thanks the Special Account for Research Grants (SARG) of the National and Kapodistrian University of Athens (NKUA) for partial support and the Bodossaki Foundation for donating the TGA to NKUA.

References

1 H.-C. Zhou, J. R. Long and O. M. Yaghi, *Chem. Rev.*, 2012, **112**, 673–674.
2 H. Furukawa, K. E. Cordova, M. O'Keeffe and O. M. Yaghi, *Science*, 2013, **341**, 1230444.
3 M. O'Keeffe and O. M. Yaghi, *Chem. Rev.*, 2012, **112**, 675–702.
4 J. A. Mason, M. Veenstra and J. R. Long, *Chem. Sci.*, 2014, **5**, 32–51.
5 D. Alezi, Y. Belmabkhout, M. Suyetin, P. M. Bhatt, Ł. J. Weseliński, V. Solovyeva, K. Adil, I. Spanopoulos, P. N. Trikalitis, A.-H. Emwas and M. Eddaoudi, *J. Am. Chem. Soc.*, 2015, **137**, 13308–13318.
6 H. Li, K. Wang, Y. Sun, C. T. Lollar, J. Li and H.-C. Zhou, *Mater. Today*, 2018, **21**, 108–121.
7 M. Eddaoudi, J. Kim, N. Rosi, D. Vodak, J. Wachter, M. O'Keeffe and O. M. Yaghi, *Science*, 2002, **295**, 469–472.
8 D.-X. Xue, Q. Wang and J. Bai, *Coord. Chem. Rev.*, 2019, **378**, 2–16.
9 J. Liu, L. Chen, H. Cui, J. Zhang, L. Zhang and C.-Y. Su, *Chem. Soc. Rev.*, 2014, **43**, 6011–6061.
10 V. P. Santos, T. A. Wezendonk, J. J. D. Jaén, A. I. Dugulan, M. A. Nasalevich, H.-U. Islam, A. Chojecki, S. Sartipi, X. Sun, A. A. Hakeem, A. C. J. Koeken, M. Ruitenbeek, T. Davidian, G. R. Meima, G. Sankar, F. Kapteijn, M. Makkee and J. Gascon, *Nat. Commun.*, 2015, **6**, 6451.
11 M. Zhao, S. Ou and C.-D. Wu, *Acc. Chem. Res.*, 2014, **47**, 1199–1207.
12 L. Jiao, Y. Wang, H.-L. Jiang and Q. Xu, *Adv. Mater.*, 2018, **30**, 1703663.
13 Y.-S. Kang, Y. Lu, K. Chen, Y. Zhao, P. Wang and W.-Y. Sun, *Coord. Chem. Rev.*, 2019, **378**, 262–280.
14 X. Li, B. Wang, Y. Cao, S. Zhao, H. Wang, X. Feng, J. Zhou and X. Ma, *ACS Sustainable Chem. Eng.*, 2019, **7**, 4548–4563.
15 S. Yuan, L. Feng, K. Wang, J. Pang, M. Bosch, C. Lollar, Y. Sun, J. Qin, X. Yang, P. Zhang, Q. Wang, L. Zou, Y. Zhang, L. Zhang, Y. Fang, J. Li and H.-C. Zhou, *Adv. Mater.*, 2018, **30**, 1704303.
16 S. Rapti, D. Sarma, S. A. Diamantis, E. Skliri, G. S. Armatas, A. C. Tsipis, Y. S. Hassan, M. Alkordi, C. D. Malliakas, M. G. Kanatzidis, T. Lazarides, J. C. Plakatouras and M. J. Manos, *J. Mater. Chem. A*, 2017, **5**, 14707–14719.
17 S. Rapti, A. Pournara, D. Sarma, I. T. Papadas, G. S. Armatas, A. C. Tsipis, T. Lazarides, M. G. Kanatzidis and M. J. Manos, *Chem. Sci.*, 2016, **7**, 2427–2436.
18 P. Kumar, A. Pournara, K.-H. Kim, V. Bansal, S. Rapti and M. J. Manos, *Prog. Mater. Sci.*, 2017, **86**, 25–74.
19 L. Zhu, D. Sheng, C. Xu, X. Dai, M. A. Silver, J. Li, P. Li, Y. Wang, Y. Wang, L. Chen, C. Xiao, J. Chen, R. Zhou, C. Zhang, O. K. Farha, Z. Chai, T. E. Albrecht-Schmitt and S. Wang, *J. Am. Chem. Soc.*, 2017, **139**, 14873–14876.
20 S. A. Diamantis, A. Margariti, A. D. Pournara, G. S. Papaefstathiou, M. J. Manos and T. Lazarides, *Inorg. Chem. Front.*, 2018, **5**, 1493–1511.
21 Z. Hu, B. J. Deibert and J. Li, *Chem. Soc. Rev.*, 2014, **43**, 5815–5840.
22 W. P. Lustig, S. Mukherjee, N. D. Rudd, A. V. Desai, J. Li and S. K. Ghosh, *Chem. Soc. Rev.*, 2017, **46**, 3242–3285.
23 Y. Zhang, S. Yuan, G. Day, X. Wang, X. Yang and H.-C. Zhou, *Coord. Chem. Rev.*, 2018, **354**, 28–45.
24 H.-R. Fu, Y. Zhao, T. Xie, M.-L. Han, L.-F. Ma and S.-Q. Zang, *J. Mater. Chem. C*, 2018, **6**, 6440–6448.
25 T. Gong, P. Li, Q. Sui, J. Chen, J. Xu and E.-Q. Gao, *J. Mater. Chem. A*, 2018, **6**, 9236–9244.
26 T. He, Y.-Z. Zhang, X.-J. Kong, J. Yu, X.-L. Lv, Y. Wu, Z.-J. Guo and J.-R. Li, *ACS Appl. Mater. Interfaces*, 2018, **10**, 16650–16659.
27 D. Banerjee, H. Wang, B. J. Deibert and J. Li, Alkaline Earth Metal-Based Metal–Organic Frameworks: Synthesis, Properties, and Applications, in *The Chemistry of Metal–Organic Frameworks: Synthesis, Characterization, and Applications*, ed. S. Kaskel, Wiley-VCH, Weinheim, 2016, vol. 1.
28 A. Douvali, G. S. Papaefstathiou, M. P. Gullo, A. Barbieri, A. C. Tsipis, C. D. Malliakas, M. G. Kanatzidis, I. Papadas, G. S. Armatas, A. G. Hatzidimitriou, T. Lazarides and M. J. Manos, *Inorg. Chem.*, 2015, **54**, 5813–5826.
29 A. Khansari, S. G. Telfer and C. Richardson, *Cryst. Growth Des.*, 2019, **19**, 268–274.
30 D. Briones, P. Leo, J. Cepeda, G. Orcajo, G. Calleja, R. Sanz, A. Rodríguez-Diéguez and F. Martínez, *CrystEngComm*, 2018, **20**, 4793–4803.
31 S. A. Diamantis, A. D. Pournara, A. G. Hatzidimitriou, M. J. Manos, G. S. Papaefstathiou and T. Lazarides, *Polyhedron*, 2018, **153**, 173–180.
32 A. Douvali, A. C. Tsipis, S. V. Eliseeva, S. Petoud, G. S. Papaefstathiou, C. D. Malliakas, I. Papadas, G. S. Armatas, I. Margiolaki, M. G. Kanatzidis, T. Lazarides and M. J. Manos, *Angew. Chem., Int. Ed.*, 2015, **54**, 1651–1656.
33 Z. H. Fard, Y. Kalinovskyy, D. M. Spasyuk, B. A. Blight and G. K. H. Shimizu, *Chem. Commun.*, 2016, **52**, 12865–12868.
34 F. Hu, Z. Di, M. Wu and J. Li, *Dalton Trans.*, 2020, **49**, 8836–8840.
35 X.-Y. Li, L.-N. Ma, Y. Liu, L. Hou, Y.-Y. Wang and Z. Zhu, *ACS Appl. Mater. Interfaces*, 2018, **10**, 10965–10973.
36 L. Asgharnejad, A. Abbasi, M. Najafi and J. Janczak, *Cryst. Growth Des.*, 2019, **19**, 2679–2686.
37 P. Leo, G. Orcajo, D. Briones, A. Rodríguez-Diéguez, D. Choquesillo-Lazarte, G. Calleja and F. Martínez, *Dalton Trans.*, 2019, **48**, 11556–11564.
38 C. Pan, J. Nan, X. Dong, X.-M. Ren and W. Jin, *J. Am. Chem. Soc.*, 2011, **133**, 12330–12333.
39 M. Usman, S. Mendiratta, S. Batjargal, G. Haider, M. Hayashi, N. Rao Gade, J.-W. Chen, Y.-F. Chen and K.-L. Lu, *ACS Appl. Mater. Interfaces*, 2015, **7**, 22767–22774.
40 R. M. P. Colodrero, P. Olivera-Pastor, E. R. Losilla, D. Hernández-Alonso, M. A. G. Aranda, L. Leon-Reina, J. Rius, K. D. Demadis, B. Moreau, D. Villemin,

M. Palomino, F. Rey and A. Cabeza, *Inorg. Chem.*, 2012, **51**, 7689–7698.
41 X.-Y. Dong, X.-P. Hu, H.-C. Yao, S.-Q. Zang, H.-W. Hou and T. C. W. Mak, *Inorg. Chem.*, 2014, **53**, 12050–12057.
42 E. Papazoi, A. Douvali, S. Rapti, E. Skliri, G. S. Armatas, G. S. Papaefstathiou, X. Wang, Z.-F. Huang, S. Kaziannis, C. Kosmidis, A. G. Hatzidimitriou, T. Lazarides and M. J. Manos, *Inorg. Chem. Front.*, 2017, **4**, 530–536.
43 Y. Lin, C. Kong and L. Chen, *RSC Adv.*, 2016, **6**, 32598–32614.
44 S. Xu and Y. Ni, *Analyst*, 2019, **144**, 1687–1695.
45 Y. Fu, D. Sun, Y. Chen, R. Huang, Z. Ding, X. Fu and Z. Li, *Angew. Chem., Int. Ed.*, 2012, **51**, 3364–3367.
46 S. Mendiratta, M. Usman, T. W. Tseng, T. T. Luo, S. F. Lee, L. Zhao, M. K. Wu, M. M. Lee, S. S. Sun, Y. C. Lin and K. L. Lu, *Eur. J. Inorg. Chem.*, 2015, **2015**, 1669–1674.
47 S. Yuan, J.-S. Qin, H.-Q. Xu, J. Su, D. Rossi, Y. Chen, L. Zhang, C. Lollar, Q. Wang, H.-L. Jiang, D. H. Son, H. Xu, Z. Huang, X. Zou and H.-C. Zhou, *ACS Cent. Sci.*, 2018, **4**, 105–111.
48 S. Kampouri, T. N. Nguyen, M. Spodaryk, R. G. Palgrave, A. Züttel, B. Smit and K. C. Stylianou, *Adv. Funct. Mater.*, 2018, **28**, 1806368.
49 C. Queirós, A. M. G. Silva, B. de Castro and L. Cunha-Silva, *Molecules*, 2020, **25**, 1353.
50 C.-X. Chen, Z. Wei, J.-J. Jiang, Y.-Z. Fan, S.-P. Zheng, C.-C. Cao, Y.-H. Li, D. Fenske and C.-Y. Su, *Angew. Chem., Int. Ed.*, 2016, **55**, 9932–9936.
51 C.-X. Chen, Z.-W. Wei, J.-J. Jiang, S.-P. Zheng, H.-P. Wang, Q.-F. Qiu, C.-C. Cao, D. Fenske and C.-Y. Su, *J. Am. Chem. Soc.*, 2017, **139**, 6034–6037.
52 R. K. Deshpande, J. L. Minnaar and S. G. Telfer, *Angew. Chem., Int. Ed.*, 2010, **49**, 4598–4602.
53 A. Khansari, M. R. Bryant, D. R. Jenkinson, G. B. Jameson, O. T. Qazvini, L. Liu, A. D. Burrows, S. G. Telfer and C. Richardson, *CrystEngComm*, 2019, **21**, 7498–7506.
54 D. J. Lun, G. I. N. Waterhouse and S. G. Telfer, *J. Am. Chem. Soc.*, 2011, **133**, 5806–5809.
55 J. Sim, H. Yim, N. Ko, S. B. Choi, Y. Oh, H. J. Park, S. Park and J. Kim, *Dalton Trans.*, 2014, **43**, 18017–18024.
56 M. S. Yazdanparast, V. W. Day and T. Gadzikwa, *Molecules*, 2020, **25**, 697.
57 M. Kaposi, M. Cokoja, C. H. Hutterer, S. A. Hauser, T. Kaposi, F. Klappenberger, A. Pöthig, J. V. Barth, W. A. Herrmann and F. E. Kühn, *Dalton Trans.*, 2015, **44**, 15976–15983.
58 M. S. Yazdanparast, V. W. Day and T. Gadzikwa, *Molecules*, 2020, **25**, 697.
59 A. T. Nielsen, A. A. DeFusco and T. E. Browne, *J. Org. Chem.*, 1985, **50**, 4211–4218.
60 M. Almáši, V. Zeleňák, R. Gyepes, Ľ. Zauška and S. Bourrelly, *RSC Adv.*, 2020, **10**, 32323–32334.
61 F. Hu, Z. Di, M. Wu and J. Li, *Dalton Trans.*, 2020, **49**, 8836–8840.
62 X.-M. Zhang, J. Lv, F. Ji, H.-S. Wu, H. Jiao and P. v. R. Schleyer, *J. Am. Chem. Soc.*, 2011, **133**, 4788–4790.
63 S. Das, H. Kim and K. Kim, *J. Am. Chem. Soc.*, 2009, **131**, 3814–3815.
64 S. Ma, D. Yuan, X.-S. Wang and H.-C. Zhou, *Inorg. Chem.*, 2009, **48**, 2072–2077.
65 H. Chun, D. Kim, D. N. Dybtsev and K. Kim, *Angew. Chem., Int. Ed.*, 2004, **43**, 971–974.
66 S. Natarajan, S. Neeraj, A. Choudhury and C. N. R. Rao, *Inorg. Chem.*, 2000, **39**, 1426–1433.
67 K. Sharma, S. K. Gupta, A. Borah and R. Murugavel, *Chem. Commun.*, 2019, **55**, 7994–7997.
68 F. Wang, Y.-B. Shu, X. Bu and J. Zhang, *Chem. – Eur. J.*, 2012, **18**, 11876–11879.
69 T. Wu, X. Bu, J. Zhang and P. Feng, *Chem. Mater.*, 2008, **20**, 7377–7382.
70 D. F. Sava, V. C. Kravtsov, J. Eckert, J. F. Eubank, F. Nouar and M. Eddaoudi, *J. Am. Chem. Soc.*, 2009, **131**, 10394–10396.
71 S. S. Mondal, A. Bhunia, A. Kelling, U. Schilde, C. Janiak and H.-J. Holdt, *Chem. Commun.*, 2014, **50**, 5441–5443.
72 Q.-R. Fang, G.-S. Zhu, Z. Jin, M. Xue, X. Wei, D.-J. Wang and S.-L. Qiu, *Angew. Chem., Int. Ed.*, 2006, **45**, 6126–6130.
73 Y.-Y. Qin, Q.-R. Ding, E. Yang, Y. Kang, L. Zhang and Y.-G. Yao, *Inorg. Chem. Commun.*, 2015, **56**, 83–86.
74 H. Reinsch, B. Bueken, F. Vermoortele, I. Stassen, A. Lieb, K.-P. Lillerud and D. De Vos, *CrystEngComm*, 2015, **17**, 4070–4074.
75 H. Hayashi, A. P. Côté, H. Furukawa, M. O'Keeffe and O. M. Yaghi, *Nat. Mater.*, 2007, **6**, 501–506.
76 M. S. Jeong, Y. Kim and K. Seff, *J. Phys. Chem.*, 1994, **98**, 1878–1881.
77 M. J. Maple, E. F. Philp, A. M. Z. Slawin, P. Lightfoot, P. A. Cox and P. A. Wright, *J. Mater. Chem.*, 2001, **11**, 98–104.
78 J. Yang, Y.-B. Zhang, Q. Liu, C. A. Trickett, E. Gutiérrez-Puebla, M. Á. Monge, H. Cong, A. Aldossary, H. Deng and O. M. Yaghi, *J. Am. Chem. Soc.*, 2017, **139**, 6448–6455.
79 V. Bon, I. Senkovska, I. A. Baburin and S. Kaskel, *Cryst. Growth Des.*, 2013, **13**, 1231–1237.
80 F. Drache, F. G. Cirujano, K. D. Nguyen, V. Bon, I. Senkovska, F. X. Llabrés i Xamena and S. Kaskel, *Cryst. Growth Des.*, 2018, **18**, 5492–5500.
81 Q.-R. Fang, D.-Q. Yuan, J. Sculley, W.-G. Lu and H.-C. Zhou, *Chem. Commun.*, 2012, **48**, 254–256.
82 N. L. Rosi, J. Kim, M. Eddaoudi, B. Chen, M. O'Keeffe and O. M. Yaghi, *J. Am. Chem. Soc.*, 2005, **127**, 1504–1518.
83 C. Serre, F. Millange, C. Thouvenot, M. Noguès, G. Marsolier, D. Louër and G. Férey, *J. Am. Chem. Soc.*, 2002, **124**, 13519–13526.
84 K. Barthelet, J. Marrot, D. Riou and G. Férey, *Angew. Chem., Int. Ed.*, 2002, **41**, 281–284.
85 V. Balzani, P. Ceroni and A. Juris, *Photochemistry and Photophysics: Concepts, Research, Applications*, Willey-VCH, Weinheim, 2014.